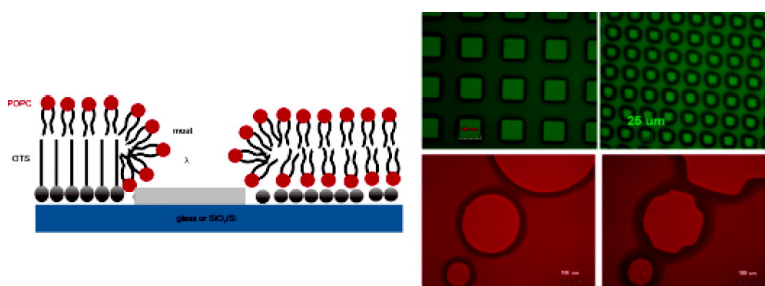Article

# Phospholipid Morphologies on Photochemically Patterned Silane Monolayers

Michael C. Howland, Annapoorna R. Sapuri-Butti, Sanhita S. Dixit,
Andrew M. Dattelbaum, Andrew P. Shreve, and Atul N. Parikh

## More About This Article

Additional resources and features associated with this article are available within the HTML version:

- Supporting Information
- Links to the 15 articles that cite this article, as of the time of this article download
- Access to high resolution figures
- Links to articles and content related to this article
- Copyright permission to reproduce figures and/or text from this article

View the Full Text HTML

# Phospholipid Morphologies on Photochemically Patterned Silane Monolayers

Michael C. Howland, Annapoorna R. Sapuri-Butti, Sanhita S. Dixit, Andrew M. Dattelbaum, Andrew P. Shreve, and Atul N. Parikh*

*Contribution from the Department of Applied Science, University of California, Davis, California 95616, and Bioscience Division, Los Alamos National Laboratory, Los Alamos, New Mexico 87545*

Received October 29, 2004;  E-mail: anparikh@ucdavis.edu

***Abstract:*** We have studied the spreading of phospholipid vesicles on photochemically patterned *n*-octadecylsiloxane monolayers using epifluorescence and imaging ellipsometry measurements. Self-assembled monolayers of *n*-octadecylsiloxanes were patterned using short-wavelength ultraviolet radiation and a photomask to produce periodic arrays of patterned hydrophilic domains separated from hydrophobic surroundings. Exposing these patterned surfaces to a solution of small unilamellar vesicles of phospholipids and their mixtures resulted in a complex lipid layer morphology epitaxially reflecting the underlying pattern of hydrophilicity. The hydrophilic square regions of the photopatterned OTS monolayer reflected lipid bilayer formation, and the hydrophobic OTS residues supported lipid monolayers. We further observed the existence of a boundary region composed of a nonfluid lipid phase and a lipid-free moat at the interface between the lipid monolayer and bilayer morphologies spontaneously corralling the fluid bilayers. The outer-edge of the boundary region was found to be accessible for subsequent adsorption by proteins (e.g., streptavidin and BSA), but the inner-edge closer to the bilayer remained resistant to adsorption by protein or vesicles. Mechanistic implications of our results in terms of the effects of substrate topochemical character are discussed. Furthermore, our results provide a basis for the construction of complex biomembrane models, which exhibit fluidity barriers and differentiate membrane properties based on correspondence between lipid leaflets. We also envisage the use of this construct where two-dimensionally fluid, low-defect lipid layers serve as sacrificial resists for the deposition of protein and other material patterns.

## Introduction

Supported phospholipid membranes (sBLMs) have been a subject of great attention because of their extraordinary ability to preserve many biophysical properties of cellular membranes.[1-3] Sustained interest in these materials can be attributed to two factors. First, they are proving to be useful platforms for modeling many reaction−diffusion processes that characterize structure, assembly, dynamics, and functions of complex, heterogeneous biological membranes.[4] Second, these material constructs promise to provide useful routes for the design of biocompatible surfaces[5,6] and biosensors for diagnosis and detection of analytes that bind to membrane targets, for example, receptor and ion-channel proteins.[7-10] Structurally, supported membranes represent a class of biomolecular interfacial films composed essentially of two opposing monolayers of phospholipids.[11,12] They are typically formed at the solid−liquid interface when vesicular microphases of lipids and their mixtures rupture and spread spontaneously on hydrophilic surfaces, but two successive transfers of lipidic monolayers from the air−water interface onto planar surfaces in Langmuir−Blodgett schemes have also been used. When appropriately formed, they are essentially separated from the substrate surface through an intervening cushion layer[13-15] of hydration water (6−15 Å thickness on silica surfaces) and exhibit two-dimensional contiguity and fluidity reminiscent of lipid membranes of vesicles and living cells.

A significant effort in the past decade has now established that substrate wettability plays an important role in determining vesicle spreading behavior[16-19] and the resulting surface-bound

(1) Sackmann, E. *Science* **1996**, *271*, 43.
(2) McConnell, H. M.; Watts, T. H.; Weis, R. M.; Brian, A. A. *Biochim. Biophys. Acta* **1986**, *864*, 95.
(3) Brian, A. A.; McConnell, H. M. *Proc. Natl. Acad. Sci. U.S.A.* **1984**, *81*, 6159.
(4) Boxer, S. G. *Curr. Opin. Chem. Biol.* **2000**, *4*, 704.
(5) Willumeit, R.; Feyerabend, F.; Kamusewitz, H.; Schossig, M.; Clemens, H. *Materialwissenschaft Und Werkstofftechnik* **2003**, *34*, 1084.
(6) Andersson, A. S.; Glasmastar, K.; Sutherland, D.; Lidberg, U.; Kasemo, B. *J. Biomed. Mater. Res., Part A* **2003**, *64A*, 622.
(7) Fang, Y.; Lahiri, J.; Picard, L. *Drug Discovery Today* **2003**, *8*, 755.
(8) Worsfold, O.; Toma, C.; Nishiya, T. *Biosens. Bioelectron.* **2004**, *19*, 1505.
(9) Cornell, B. A.; BraachMaksvytis, V. L. B.; King, L. G.; Osman, P. D. J.; Raguse, B.; Wieczorek, L.; Pace, R. J. *Nature* **1997**, *387*, 580.
(10) Bayley, H.; Cremer, P. S. *Nature* **2001**, *413*, 226.

(11) Tamm, L. K. *Klinische Wochenschrift* **1984**, *62*, 502.
(12) Tamm, L. K.; McConnell, H. M. *Biophys. J.* **1985**, *47*, 105.
(13) Johnson, S. J.; Bayerl, T. M.; McDermott, D. C.; Adam, G. W.; Rennie, A. R.; Thomas, R. K.; Sackmann, E. *Biophys. J.* **1991**, *59*, 289.
(14) Gutberlet, T.; Steitz, R.; Fragneto, G.; Klosgen, B. *J. Phys.: Condens. Matter* **2004**, *16*, S2469.
(15) Koenig, B. W.; Kruger, S.; Orts, W. J.; Majkrzak, C. F.; Berk, N. F.; Silverton, J. V.; Gawrisch, K. *Langmuir* **1996**, *12*, 1343.
(16) Lipowsky, R.; Seifert, U. *Mol. Cryst. Liq. Cryst.* **1991**, *202*, 17.
(17) Seifert, U.; Lipowsky, R. *Phys. Rev. A* **1990**, *42*, 4768.
(18) Twardowski, M.; Nuzzo, R. G. *Langmuir* **2003**, *19*, 9781.

lipidic phases. At hydrophilic surfaces,[20] exposure of small unilamellar vesicles generally results in rupture and spreading of phospholipid vesicles, forming single phospholipid bilayers. Examples include freshly oxidized surfaces of glass, quartz, mica, and silicon wafers. Hydrophobic supports,[19,21−24] on the other hand, foster vesicle spreading by a notably different mechanism which consistently produces single phospholipid monolayers. Here, cases studied include low-energy methyl (CH₃) surfaces (critical surface tension values of 20−22 D/cm[25]) of self-assembled organic monolayers of alkanethiols[23,26] and alkylsiloxanes[22] as well as Langmuir−Blodgett films of single phospholipid monolayers.[27] In this regard, studies aimed at examining how vesicle spreading occurs on support surfaces that display heterogeneity of surface hydrophilicities are lacking.[28] We reasoned that if vesicle spreading mechanisms respond directly to local and spatial variations in surface energies (or wettabilities), then it should be possible to construct surfaces that display monolayers and bilayers of phospholipids juxtaposed on a single substrate surface. Such composite surfaces would potentially be of significant interest as useful models for direct comparisons of membrane functions that require correspondence between the two leaflets of the bilayer architecture. Furthermore, many hydrophilic surfaces used for bilayer formation are easily contaminated by adventitious organics[29] and thus display surface chemical and wettability heterogeneities.

Here, we investigate vesicle spreading behavior on binary surfaces displaying patterns of hydrophilic regions within hydrophobic surroundings. Our results show that the resulting surfaces display three distinct lipid film morphologies that reflect the underlying pattern. We confirm the formation of fluid bilayers in hydrophilic parts of the substrate and of single monolayers on the hydrophobic parts of the surface. Our data reveal a complex morphology comprising a lipid-free gap separating the bilayer from the monolayer morphology at the substrate interface between the hydrophilic and the hydrophobic domain. In many instances, the moat between the monolayer and bilayer also displays an additional nonfluid lipid phase comprising presumably sparsely distributed unfused vesicles or their fragments. New mechanistic insights that can be gleaned from the present results and the practical application of the approach in designing spontaneously corralled lipid bilayer arrays are also discussed.

## Experimental Section

**Materials.** 1-Palmitoyl-2-oleoyl-*sn*-glycero-3-phosphocholine (POPC), 1,2-dilauroyl-*sn*-glycero-3-phosphocholine (DLPC), and 1,2-dimyris-toyl-*sn*-glycero-3-phosphocholine (DMPC) phospholipids were pur-

chased from Avanti Polar Lipids (Birmingham, AL). Texas Red 1,2-dihexadecanoyl-*sn*-glycero-3-phosphoethanolamine, triethylammonium salt (TR), *N*-(7-nitrobenz-2-oxa-1,3-diazol- 4-yl)-1,2-dihexadecanoyl-*sn*-glycero-3-phosphoethanolamine, triethylammonium salt (NBD-PE, tail-labeled), 2-(6-(7-nitrobenz-2-oxa-1,3-diazol-4-yl)amino)hexanoyl-1-hexadecanoyl-*sn*-glycero-3-phosphocholine (NBD C₆-HPC, head-labeled), Lissamine rhodamine B 1,2-dihexadecanoyl-*sn*-glycero-3-phosphoethanolamine, triethylammonium salt (rhodamine DHPE), and 1,1′-dioctadecyl-3,3,3′,3′-tetramethylindocarbocyanine perchlorate (DiIC18(3)) probes were used as purchased from Molecular Probes (Eugene, OR). The proteins, streptavidin, and bovine serum albumin, labeled with fluorescein-5-isothiocyanate (FITC), were acquired from Molecular Probes. All lipids were suspended and stored in chloroform or chloroform/alcohol mixture in the freezer (−20 °C) until used. Hydrogen peroxide (30% v/v) and sulfuric acid were purchased from J. T. Baker (Phillipsburg, NJ) and Fisher Chemicals (Fairlawn, NJ), respectively, and used as received. All organic solvents were HPLC grade. All chemicals were used without further purification. Organic-free deionized water of high-resistivity (approximately 18.0 mΩ·cm) was obtained by processing water first through a reverse osmosis deionization unit and then a Milli-Q Plus water unit (Model ZD40-11595, Bedford, MA) consisting of a five-bowl purification system (equipped with two Ion-Ex, one Super-C, one Organex-Q, and an additional ultrafiltration cartridge). Phosphate buffer saline (PBS, pH 7.2, 154 mM NaCl, 1.54 mM KH₂PO₄, and 2.71 mM Na₂HPO₄) was obtained from Gibco-Life technology (Rockville, MD) and used as vesicle spreading solution and buffer media. Corning glass coverslips (No. 1 1/2 and 2, 22 and 18 mm², respectively, Fisher HealthCare, Houston, TX) were used as substrates unless noted otherwise. Silicon substrates with native oxide overlayers (Silicon Sense, Nashua, NH) were used for ellipsometry measurements. Selected experiments used silicon substrates with 100 nm oxide (Silicon Sense, Nashua, NH) to allow ellipsometry and fluorescence measurements on single substrates.

**Substrate Preparations.** The substrates (silicon oxide wafers or Corning glass coverslips) were cleaned from adventitious contaminants[29] by oxidizing in a freshly prepared 4:1 (v/v) mixture of sulfuric acid and hydrogen peroxide for a period of 4−5 min maintained at ∼100 °C (*Caution: this mixture reacts violently with organic materials and must be handled with extreme care*). The substrates were then withdrawn using Teflon tweezers, rinsed immediately with a copious amount of deionized water, and dried in a stream of nitrogen. All cleaned, oxidized substrates were used within 1 day of the pretreatment.

**Surface Derivatizations using *n*-Octadecyltrichlorosilane.** All freshly oxidized, dry SiO₂/Si, silicon substrates with thermally grown oxides, and coverglass substrates were immersed in a 50 mL self-assembly solution consisting of 2.5 mM octadecyltrichlorosilane (CH₃-(CH₂)17SiCl₃, OTS) (90% Aldrich) solution in anhydrous hexadecane (99% Sigma-Aldrich).[25] The substrates were allowed to incubate with the self-assembly solution for approximately 45 min. All silanization reactions were carried out in glass containers under nominally dry ambient conditions (relative humidity <20%). All the reaction vessels used were thoroughly precleaned using Alconox detergent followed by extensive washing with deionized, low organic water and finally air-dried in an oven. After removal from the self-assembly solution, the film-covered wafers were washed extensively with chloroform under ultrasonic conditions to remove all excess reactants. Silanized samples were used within a few days of preparation.

**UV Photolithography of *n*-Octadecylsiloxane Monolayers.** Spatial patterning of OTS-covered substrates was achieved using short-wavelength UV radiation.[30,31] In particular, spatially directed photo-illumination of monolayer samples was achieved using a physical mask and an ozone-generating UV lamp.[32] The masks displaying patterns of

(19) Silin, V. I.; Wieder, H.; Woodward, J. T.; Valincius, G.; Offenhausser, A.; Plant, A. L. *J. Am. Chem. Soc.* **2002**, *124*, 14676.
(20) Nissen, J.; Gritsch, S.; Wiegand, G.; Radler, J. O. *Eur. Phys. J. B* **1999**, *10*, 335.
(21) Radler, J.; Strey, H.; Sackmann, E. *Langmuir* **1995**, *11*, 4539.
(22) Parikh, A. N.; Beers, J. D.; Shreve, A. P.; Swanson, B. I. *Langmuir* **1999**, *15*, 5369.
(23) Plant, A. L. *Langmuir* **1999**, *15*, 5128.
(24) Hubbard, J. B.; Silin, V.; Plant, A. L. *Biophys. Chem.* **1998**, *75*, 163.
(25) Parikh, A. N.; Allara, D. L.; Azouz, I. B.; Rondelez, F. *J. Phys. Chem.* **1994**, *98*, 7577.
(26) Plant, A. L.; Gueguetchkeri, M.; Yap, W. *Biophys. J.* **1994**, *67*, 1126.
(27) Kalb, E.; Frey, S.; Tamm, L. K. *Biochim. Biophys. Acta* **1992**, *1103*, 307.
(28) One previous study by Jenkins and co-workers (Jenkins, A. T. A.; Bushby, R. J.; Evans, S. D.; Knoll, W.; Offenhausser, A.; Ogier, S. D. *Langmuir* **2002**, *18*, 3176−3180) used micropatterned monolayers of alkanethiols to design a chemically patterned surface. Using scanning probe microscopy and surface plasmon microscopy measurements, they concluded a significantly complex response of egg-PC vesicles at these surfaces and noted gross inconsistencies in the vesicle spreading mechanisms.
(29) Frantz, P.; Granick, S. *Langmuir* **1992**, *8*, 1176.
(30) Dulcey, C. S.; Georger, J. H.; Krauthamer, V.; Stenger, D. A.; Fare, T. L.; Calvert, J. M. *Science* **1991**, *252*, 551.
(31) Jonas, U.; del Campo, A.; Kruger, C.; Glasser, G.; Boos, D. *Proc. Natl. Acad. Sci. U.S.A.* **2002**, *99*, 5034.

chrome over quartz substrate were either acquired from Photoscience, Inc. (Torrance, CA) or produced at the UC Davis Microfabrication Facility.[33] On selective masks, the edges of the chrome were deliberately roughened by over-exposure of the protective photoresist layer prior to etching of the chrome. UV radiation was produced using a medium-pressure Hg-discharge grid lamp (UVP, Inc., Upland, CA) in a quartz envelope and maintained in a closed chamber in a chemical hood. The samples were placed in contact with the photomask and positioned approximately 0.5−2 mm from the light source depending on the illumination geometry. (*Caution: direct exposure to short-wavelength UV light (187 nm, 254 nm) must be avoided, and appropriate eyewear must be worn. Care must be taken in venting the ozone by operating grid lamps under chemical hoods. The breathing of ozone in high concentrations is dangerous. Ozone concentration in excess of 0.1 ppm can cause irritation.*) The exposure period was approximately 40−60 min depending on the exposure geometry (sample−lamp distance) and the age of the lamp. Following the exposure, the mask was separated from the substrate surface, samples rinsed thoroughly using water, chloroform, and ethanol, and dried with nitrogen. Patterned OTS samples were used within 24 h of preparation.

**Vesicle Spreading on Patterned OTS Surfaces.** Supported phospholipid bilayers were formed primarily using previously reported vesicle fusion and rupture method.[11,34,35] Briefly, small unilamellar vesicles (SUVs) were prepared using vesicle extrusion methods.[36] Typically, a desired amount of lipid or lipid mixtures suspended in chloroform or chloroform/methanol mixtures was mixed in a glass vial. The solvent phase was then evaporated under a stream of nitrogen and subsequently evacuated for at least 1 h in a vacuum desiccator. The dried lipid mixture was then suspended in Millipore water and kept at 4 °C to be rehydrated overnight. The total lipid concentration was 2 mg/mL. Dye concentrations were 1 mol % for stocks containing Texas Red, 0.25 mol % for rhodamine, 3 mol % for those containing either head- or tail-labeled NBD and 1 mol % for DiIC18. The desired amount of hydrated aqueous solution was then sonicated and passed through a Avanti Mini-Extruder (Avanti, Alabaster, AL) using 0.1 $\mu$m polycarbonate membrane filters (Avanti, Alabaster, AL) for 21 times at a desired temperature (typically 10 °C above the transition temperature for the major lipids). One part of the resulting SUV solutions was diluted with one part of PBS and stored at 4 °C until use. The SUV solutions were used within a day.

Vesicle spreading was carried out by placing the substrates over a ∼80 $\mu$L SUV drop placed at the bottom of a crystallization well. The samples were allowed to incubate for 10−30 min to ensure equilibrium coverage. OTS-coated hydrophobic surfaces used in control experiments were incubated for at least 30 min. The well was then filled with water and transferred to a large reservoir of water in which the substrate was shaken gently to remove excess lipids. Finally, the substrates were transferred to culture wells making sure that the substrates *remain submerged in water*. Supported bilayer samples prepared in this way were then stored in deionized water or PBS buffer for further characterization.

**Langmuir−Blodgett Assembly of Lipid Layers.** Selected samples were prepared using a Langmuir−Blodgett procedure. Langmuir monolayers of lipid were prepared on a computer-controlled, Langmuir trough (Model 611, NIMA Technologies, Coventry, England) made of poly(tetrafluoroethylene) (PTFE). The moving barriers were Teflon-

coated, and the surface pressure (Π) measurements were made by the Wilhelmy plate method using a 21 mm perimeter plate cut from a filter paper.

The trough was first thoroughly cleaned with chloroform and ethanol (99.99% Aldrich, Milwaukee, WI) and then rinsed with Millipore filtered water. After aspiration of the rinse water, the trough was filled with fresh Millipore water for use as a subphase. A patterned OTS substrate was submerged vertically into the trough before application of lipid molecules. The backside was typically protected with a thin film of poly(dimethylsiloxane) (PDMS) (Dow Corning Corporation, Midland, MI) to ensure single-sided deposition. To generate a monolayer, 50 $\mu$L of lipid in chloroform was spread dropwise onto a subphase of Millipore filtered water. Thirty minutes were allowed for the solvent to evaporate before monolayer compression. The monolayer was compressed to desired surface pressures (20−35 mN/m) by decreasing the trough area at 40 cm$^2$/min. Once the target pressure was achieved, the surface was allowed to re-equilibrate for 30 min. The substrate was then drawn upward at 5 mm/min. After removal of the substrate, the PDMS was peeled off and the dipper clip was replaced with an adhesive agent, allowing for horizontal attachment of the substrate to the dipper arm. The pressure was maintained at the initial value (20−35 mN/m), and the substrate was pushed horizontally back through the monolayer a 5 mm/min. The sample was then removed from the dipper and captured in the subphase. The trough surface was then aspirated. The sample remained submerged when removed from the subphase.

**Epifluorescence Microscopy.** A Nikon eclipse TE2000-S inverted fluorescence microscope (Technical Instruments, Burlingame, CA) equipped with an ORCA-ER (Model LB10-232, Hamamatsu Corporation, Bridgewater, NJ) or Retiga-1300 CCD camera (Technical Instruments, Burlingame, CA) and a Hg lamp as the light source was used to visualize all fluorescent samples. Two filter wheels, one containing a set of excitation and the other emission filters, were mounted in front of the light source and the CCD camera, respectively. An extra triple-band emitter was installed in the dichroic mirror cube for aiding in focusing through the eyepiece. Typically, images taken were using a Plan 10X (NA, 0.25) or a Plan Fluor, ELWD 20X (NA, 0.45) objectives (Nikon, Japan). High-resolution images were obtained using 60X (NA, 0.7) objectives. Images were stored and processed using simple PCI software (Compix, Inc., Cranberry Township, PA) augmented with a quantitative dynamic intensity analysis module. Fluorescence images taken with the Texas Red filter set were assigned the color red, and the images acquired with the FITC filters were assigned the color green. Excitation and emission maxima for the probes used were 583/601 nm for TR-DHPE, 463/536 nm for NBD-DHPE, 560/581 nm for rhodamine-DHPE, and 549/565 nm for DiIC18.

To characterize membrane fluidity, a simple method to assess fluorophore mobility within the membrane media was employed. We used microscopy-based fluorescence photobleach recovery measurements by adapting the circular spot photobleaching method.[37,38] Here, a circular region of the fluorescent bilayer sample, ∼30−50 $\mu$m diameter, was illuminated at high power continuously at the excitation wavelength for the fluorophore through a Plan Fluor, ELWD 60X (NA, 0.70) objective for ∼2 min. The exposure bleaches a dark spot on the bilayer caused by the photoexcitation of the fluorophore followed by an irreversible chemical transformation effected by its reaction with oxygen dissolved in the ambient buffer. After photobleaching, the illumination path was replaced by a low-power observation beam through a 10X objective to record wide-field images of fluorescence recovery in the bleached area at 30 s intervals. The subsequent lateral motion of unperturbed fluorophore−lipids from the unbleached background into the bleached spot (and vice versa) is recorded in the recovery profiles. It has been previously established that the precise shape of the recovery curve can be used to qualitatively characterize

(32) Vig, J. R. *J. Vac. Sci. Technol., A* **1985**, *3*, 1027.
(33) The latter photomasks, consisting of 1000 Å of e-beam-evaporated (CHA Industries, Fremont, CA) chrome onto a 200 $\mu$m thick double-side polished quartz wafer (Hoffman Materials, Carlisle, PA), were made in a class 100 clean room. Shipley 1813 positive photoresist (Microchem, Newton, MA) was patterned using a Karl Suss aligner. Exposed chrome was then etched away in a room temperature chromium etch bath followed by removal of the remaining photoresist.
(34) Cremer, P. S.; Boxer, S. G. *J. Phys. Chem. B* **1999**, *103*, 2554.
(35) Bayerl, T. M.; Bloom, M. *Biophys. J.* **1990**, *58*, 357.
(36) Mayer, L. D.; Hope, M. J.; Cullis, P. R. *Biochim. Biophys. Acta* **1986**, *858*, 161.

(37) Wolf, D. E. *Methods Cell Biol.* **1989**, *30*, 271.
(38) Axelrod, D.; Koppel, D. E.; Schlessinger, J.; Elson, E.; Webb, W. W. *Biophys. J.* **1976**, *16*, 1055.

the nature of the fluorophore motion.[38] Furthermore, for diffusion-like motions, the measurements of the time required for the fluorescence intensity to recover halfway ($t_{1/2}$) between its immediate post-bleach value and its long-time asymptotic value were used to estimate the diffusion coefficient, $D$, a measure of the fluidity of the lipid environment.[39] Specifically, we followed a simplified method reported by Yguerabide et al.[40] which approximates the solution of two-dimensional lateral diffusion equation using a modified Bessel function. Here, the experimental fluorescence intensity versus time data are replotted as reduced intensity versus time. The reduced intensity is given by $I$ (red) $= [I(\infty) - I(t)]/[I(\infty) - I(0)]$, where $I(t)$, $I(0)$, and $I(\infty)$ correspond to fluorescence intensity at time $t$ after photobleaching, immediately after photobleaching, and long-time asymptotic recovery values, respectively. The plot is then used to estimate $t_{1/2}$ which is, in turn, used to calculate $D = 0.22\ r_0^2/t_{1/2}$, where $r_0$ refers to the initial size of the photobleached spot. Note that the exposure time ($\sim$2 min) required in objective-based photobleaching introduces some bilayer fluidity-dependent inaccuracies in the measurements of exact diffusion constants for probe lipids.

**Imaging Ellipsometry.** Ellipsometric angle measurements[41] and spatially resolved ellipsometric contrast images[42−44] were acquired using an Elli2000 imaging system (Nanofilm Technologie, Göttingen, Germany). The ellipsometer employed a frequency-doubled Nd:YAG laser (adjustable power up to 20 mW) at 532 nm and equipped with a motorized goniometer for an accurate selection of the incidence angle and corresponding detector positions. The ellipsometer employed the typical PCSA (polarizer−compensator−sample−analyzer) nulling configuration in which a linear polarizer (P) and a quarter-wave plate (C) yield an elliptically polarized incident beam. Upon reflection from the sample (S), the beam is gathered via an analyzer (A) and imaged onto a CCD camera through a long working distance 10X objective. The P, C, and A positions that yielded the null condition are then converted to the ellipsometric angles, $\Delta$ and $\psi$. Measurements were generally taken at an incidence angle of 60°. *Silicon substrates with native oxide overlayer (SiO$_2$/Si) whose surface chemistry is comparable to that of glass were used to enhance the optical contrast with the lipid phase. For characterization under aqueous conditions, a fluid cell was used (Nanofilm Technologie, Göttingen, Germany). The cell consisted of a Teflon chamber ($\sim$3 mL volume) with glass windows fixed at 60° (incidence angle) to the substrate normal.*

Topographical maps of $\Delta$ were generated using the micromapping feature of the Elli2000 software suite. The method used assumes that $\psi$ is constant. In our specific experimental configuration and the sample systems, this assumption was accurate. Typically, 70 contrast images were scanned incrementally over a 2° change in polarization angle, while maintaining the analyzer angle at a constant value. These scans were then assembled to determine the null for each point comprising 2 × 2 pixel binning. $\Delta$ values estimated for the individual null conditions were mapped two-dimensionally. These maps were then transferred to a computer as ASCII files from which the final images were constructed using a commercial plotting software (SigmaPlot, SPSS Inc., Chicago, IL). Spatially resolved ellipsometric thicknesses were calculated from $\Delta$ values using commercial modeling software employing parallel slab model and standard electromagnetic theory. Measurements were conducted using SiO$_2$/Si substrates. A four-component (Si, SiO$_2$, organic layer(s), and ambient) parallel slab model assuming infinite substrate and ambient phases was used. Refractive indices were assumed to be $4.1502 + 0.0449i$, $1.4608 + 0.0i$, $1.45 +$

$0.0i$, and $1.0000 + 0.0i$ for silicon, silicon dioxide, organic film, and air, respectively. When samples were characterized under water, the ambient was changed to $1.332 + 0.0i$.

## Results

**Formation and Patterning of the OTS Monolayer.** Spontaneous self-assembly of OTS molecules on oxidized silicon (SiO$_2$/Si) and glass substrates gave rise to substrate autophobicity. The essentially dry emergence of the substrates from the self-assembly solution was the first evidence for the formation of high-quality OTS monolayers.[45] Routine applications of single-wavelength ellipsometry yielded a quick and convenient assessment of the film quality. An analysis of ellipsometric angles using standard electromagnetic theory yielded an optical thickness of $\sim$26 ($\pm$2) Å, in excellent agreement with previous studies. The most extensive studies of ellipsometric thickness of alkylsiloxane films are those of Wasserman et al.[46] who report a range of values between 22.6 and 27.6 Å for high-coverage OTS films prepared on oxidized silicon wafers. On the basis of the ideal limiting film thickness of 26.2 Å based on the length of the fully extended OTS chain, the current values represent the near-limiting packing density of OTS molecules. At these densities, the molecules orient along the surface normal, thereby displaying chain-terminal CH$_3$ groups at the ambient interface. Furthermore, the presentation of high-density CH$_3$ group lattice at the ambient interface makes the surface highly hydrophobic. Indeed, previous studies employing rigorous contact angle measurements have suggested the values of 20−21 D/cm for a high-quality OTS monolayer.[47] Our preliminary measurements using water contact angles (>110°) are consistent with these findings and confirm the formation of uniform surfaces of high hydrophobicity.

It is now well-appreciated that deep UV irradiation of silica surfaces results in photodesorption of organic contaminants and adsorbates and results in clean oxide surfaces of high hydrophilicity.[30] To determine if the UV-induced photochemical patterning resulted in the controlled introduction of hydrophilic regions within the hydrophobic OTS monolayer, we carried out a simple condensation test. The condensation of a vapor to a liquid on a cold surface that is not fully wetted by that liquid gives rise to an array of liquid droplets which reflect the underlying pattern of interfacial free energy (and hence substrate wettability).[48] Exposure to warm moist air, including simple breath-tests, revealed a well-defined pattern of water droplets on the UV-patterned OTS surfaces. An optical image of a water droplet on a 250 $\mu$m hydrophilic void on a patterned OTS monolayer shown in Figure 1b confirms the presence of hydrophilic regions on the OTS-coated silica surfaces where UV illumination occurred. Also shown in Figure 1a is a bright-field image of the photomask for comparison. These results are entirely consistent with previous studies which suggest the formation of patterned hydrophilicity surfaces upon localized removal of OTS monolayers from silica surfaces in masked UV exposures.[31]

Ellipsometric contrast imaging provided a more rigorous examination of the film morphologies. A representative two-

(39) Lee, G. M.; Jacobson, K. *Cell Lipids* **1994**, *40*, 111.
(40) Yguerabide, J.; Schmidt, J. A.; Yguerabide, E. E. *Biophys. J.* **1982**, *40*, 69.
(41) Aspnes, D. E. *Surf. Sci.* **1980**, *101*, 84.
(42) Neumaier, K. R.; Elender, G.; Sackmann, E.; Merkel, R. *Europhys. Lett.* **2000**, *49*, 14.
(43) Albersdorfer, A.; Elender, G.; Mathe, G.; Neumaier, K. R.; Paduschek, P.; Sackmann, E. *Appl. Phys. Lett.* **1998**, *72*, 2930.
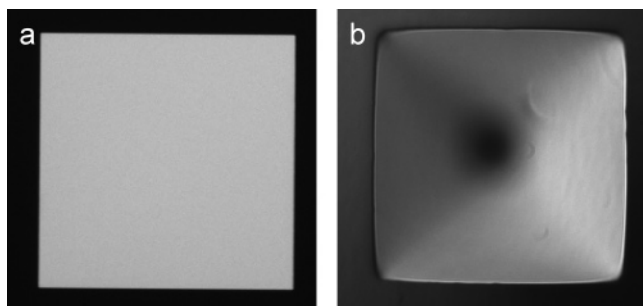(44) Reiter, R.; Motschmann, H.; Orendi, H.; Nemetz, A.; Knoll, W. *Langmuir* **1992**, *8*, 1784.

(45) Netzer, L.; Sagiv, J. *J. Am. Chem. Soc.* **1983**, *105*, 674.
(46) Wasserman, S. R.; Whitesides, G. M.; Tidswell, I. M.; Ocko, B. M.; Pershan, P. S.; Axe, J. D. *J. Am. Chem. Soc.* **1989**, *111*, 5852.
(47) Brzoska, J. B.; Shahidzadeh, N.; Rondelez, F. *Nature* **1992**, *360*, 719.
(48) Lopez, G. P.; Biebuyck, H. A.; Frisbie, C. D.; Whitesides, G. M. *Science* **1993**, *260*, 647.

**Figure 1.** A bright-field optical image of the mask with 250 $\mu$m × 250 $\mu$m square (a) and corresponding image of a square water droplet atop the OTS monolayer patterned using the mask (b).

dimensional thickness map derived from spatially resolved ellipsometric angles is shown in Figure 2. The image was for an OTS sample photopatterned using a photomask displaying 100 $\mu$m × 100 $\mu$m square features transparent to the UV radiation. These data clearly show the presence of well-defined depressions in film thickness by ~2.3 nm in square regions where illumination occurred. A cross-section of the film along the central depression in Figure 2 is shown as an inset. Here, the width of the depression and change in film thickness with respect to the OTS background are easily noted. Dulcey et al.[30] have previously suggested that the photochemical oxidation of silane monolayers results in bond cleavage at the Si—C bond followed by further fragmentation of the organic residue into volatile components which escape the silica surface leaving behind $SiO_x$ residues at the surface.[49] Our observations of depressions in monolayer thickness by ~2.3 nm, in comparison with the estimated film thickness of 2.6 nm, suggest that an approximately 0.3 nm residue is left behind at the hydrophilic surface. These values correspond well with a monolayer thickness of $SiO_x$, in agreement with the model above.

Taken together, the evidence above establishes that the photochemically patterned OTS surfaces result in mixed hydrophilicity surfaces that also exhibit a 2.3 nm topographic corrugation, presumably by highly localized and complete degradation of alkyl chains in the regions of UV exposure.

**Self-Assembly of Phospholipids on Patterned Monolayer Surfaces.** A combination of epifluorescence imaging, fluorescence photobleach recovery, and imaging ellipsometry measurements was used to determine the physical properties of the self-assembled phospholipid layers on photopatterned OTS surfaces. These results are presented below.

**Fluorescence Microscopy.** A representative example of an epifluorescence emission image for POPC bilayers deposited on patterned OTS surfaces is shown in Figure 3a. To enable fluorescence visualization, the starting vesicles were doped with a 1 mol % Texas Red DHPE probe. Template OTS patterns comprised of 100 $\mu$m × 100 $\mu$m square regions, where photochemical degradation of the OTS monolayer occurred. A high-contrast fluorescent pattern comprising three regions of distinctly different fluorescence intensities is immediately discerned: (1) bright and homogeneous fluorescent region within the pattern squares; (2) weaker, yet homogeneously fluorescent, background region; and (3) a dark rim separating the two regions above, essentially devoid of fluorescence emission.

A careful examination of the fluorescence patterns observed above highlights many salient features of these patterns. First, correlations between the observed fluorescence pattern and the initial pattern of OTS surface structure can be determined by comparing the fluorescence pattern (Figure 3b), the corresponding bright-field image of the photomask (Figure 3a) used to pattern OTS monolayers, and the ellipsometric image of the patterned OTS monolayer on oxidized silicon substrates (Figure 2). The comparison reveals a close correspondence. The patterns in fluorescence images correspond directly to the patterns of surface hydrophilicity and topography generated by UV patterning of silane monolayers. In particular, the exposed region during UV patterning, corresponding to quartz (UV transparent) regions of the mask and where OTS molecules photochemically desorbed correspond to high intensity, shows homogeneous fluorescence due to the probe-doped lipid layer. By contrast, the unexposed (UV opaque) regions associated with chrome patterns of the mask and where the OTS molecules were inferred to remain providing a hydrophobic surface exhibit a weaker, albeit homogeneous, fluorescence. We also note the emergence of the moat region displaying an essentially fluorescence-free boundary at the interface between the UV-exposed (hydrophilic) and UV-protected (hydrophobic) parts of the OTS sample. Several previous studies[1] have established that vesicles fuse on hydrophilic surfaces to form single bilayers,[50] whereas the spreading of vesicles onto hydrophobic surfaces results in a monolayer of lipids.[27] Our observations of fluorescence intensity contrasts in the hydrophilic and hydrophobic regions of the substrate are consistent with this picture. The existence of the moat region at the boundaries could not be predicted based on available data in the literature. Tentatively, we assign this region to be resistant to lipid adsorption. Later in the paper, a more detailed characterization is afforded by reconciling several different lines of evidence gathered in this study.

Second, a comparison of the spatial variations in fluorescence intensity shown in Figure 3b reveals that the fluorescence intensity in each of the three regions is essentially constant at uniform values above the lowest value recorded, and that the relative intensities in the two fluorescent regions are ~1.72: 1.0. *Average values derived from more than 30 independent samples yielded the intensity ratios of 1.87:1.* These ratios further support the notion that a full bilayer, with twice the population of fluorophore (and hence presumably the lipid), is formed at the hydrophilic sites of the patterned OTS surface compared to a lipid monolayer formed at the hydrophobic regions of the sample. *We believe that the departure from the expected 2:1 intensity ratio may reflect small variations in molecular densities between the mono- and the bilayer configurations. However, given the semiquantitative nature of our measurements, this scenario cannot be conclusively established.* Figure 4 shows epifluorescence images and real intensity histograms (Figure 4a,b) for fluorescence emission patterns observed when *thermally oxidized* silicon (oxide thickness = 100 nm) wafers were used as substrates. These images provide additional information regarding the finer lipid structure in the interface region between the hydrophilic and the hydrophobic areas of the patterned sample. Specifically, the real histograms clearly reveal that the moat is not monolithic. It reveals the presence of nonvanishing fluorescence intensity closer to the

(49) Ouyang, M.; Yuan, C.; Muisener, R. J.; Boulares, A.; Koberstein, J. T. *Chem. Mater.* **2000**, *12*, 1591.

(50) Johnson, J. M.; Ha, T.; Chu, S.; Boxer, S. G. *Biophys. J.* **2002**, *83*, 3371.
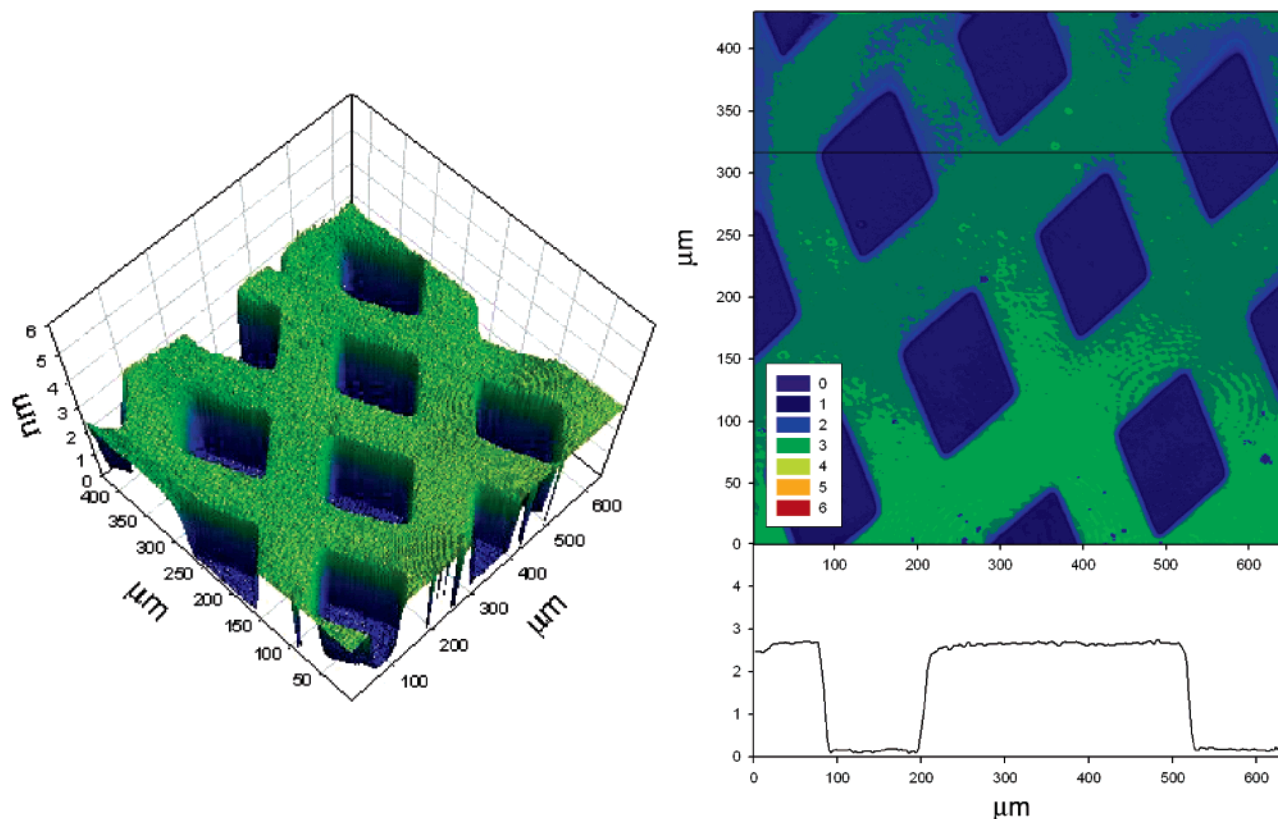
**Figure 2.** Spatially resolved ellipsometric contrast image of a UV-patterned dry OTS film displaying a 100 $\mu$m $\times$ 100 $\mu$m square void in the OTS monolayer obtained using a 10X objective and 2 $\times$ 2 pixel binning (see text for details). Inset shows a line section along the direction indicated by an arrow.
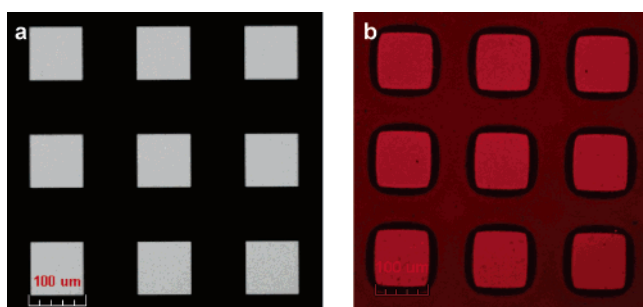


**Figure 3.** A bright-field image of the photomask showing a 100 $\mu$m $\times$ 100 $\mu$m UV transparent squares pattern separated by 100 $\mu$m distance in a chrome surrounding. Figure 3b shows an epifluorescence image of a supported bilayer (1% Texas Red, 99% POPC) formed by vesicle fusion on similarly patterned OTS monolayer.

lipid monolayer edge (exterior moat) and a virtually fluorescence-free region closer to the bilayer edge (interior moat). Preliminary fluorescence photobleach recovery (FPR) measurement in the vicinity of the exterior moat revealed little or no recovery, suggesting that any lipidic phase in this region must be nonfluid. On the basis of these preliminary observations, it appears to be plausible that irreversibly adsorbed free fluorophores or a low-density distribution of unfused vesicles or their fragments adhere in the exterior moat region. Further characterization of the moat region is important due to its unique protein adsorption characteristics (see below) and will be separately reported.

Third, a closer examination of the images using high-magnification objectives (60X, 0.7 NA, Supporting Information) shows that while sharp edges separate the fluorescent and dark regions, sharp corners of geometrical features on the mask always resulted in smoothly curved or rounded edges. This

rounding-off was absent in the masks used but was consistently seen in the lipid morphologies, as revealed by the epifluorescence emissions and ellipsometric characterization. We attribute the edge-smoothening to steric forces and line tension effects. We also note that the sizes of the essentially fluorescence-free moat regions depended most critically on the distance between the sample and the mask. When the mask was maintained at an inclination relative to the substrate surface, the sizes varied continuously from one side to the other side of the sample (Supporting Information). Careful attention to sample handling and mask contact was shown to reduce the size and increase the regularity of the rim,[51] though we were unable to eliminate the rim even when the sample was pressed to the mask during patterning. These controls suggest that the exterior part of the moat closer to the lipid monolayer is at least partially formed due to edge effects associated with the previously suggested penumbral blurring in the masked lithography of the original OTS monolayer.[52,53]

Examples presented in Figure 5 illustrate the broader generality of the approach. Hydrophilic features of various sizes, shapes, and distributions could be patterned within the OTS monolayer. Vesicle spreading in all cases gave rise to three-intensity level fluorescence patterns. The smallest sizes we produced were 25 $\mu$m, separated by 25 $\mu$m center-to-center separation, covering the entire sample surface (e.g., 22 $\times$ 22 mm$^2$ coverglass), and we were only limited by the size of the mask or the substrate

(51) In many samples, the rim itself was also observed to consist of two regions of low fluorescence intensity.
(52) Hong, L.; Sugimura, H.; Takai, O.; Nakagiri, N.; Okada, M. *Jpn. J. Appl. Phys.* **2003**, *42*, L394.
(53) Sugimura, H.; Saito, N.; Maeda, N.; Ikeda, I.; Ishida, Y.; Hayashi, K.; Hong, L.; Takai, O. *Nanotechnology* **2004**, *15*, S69.
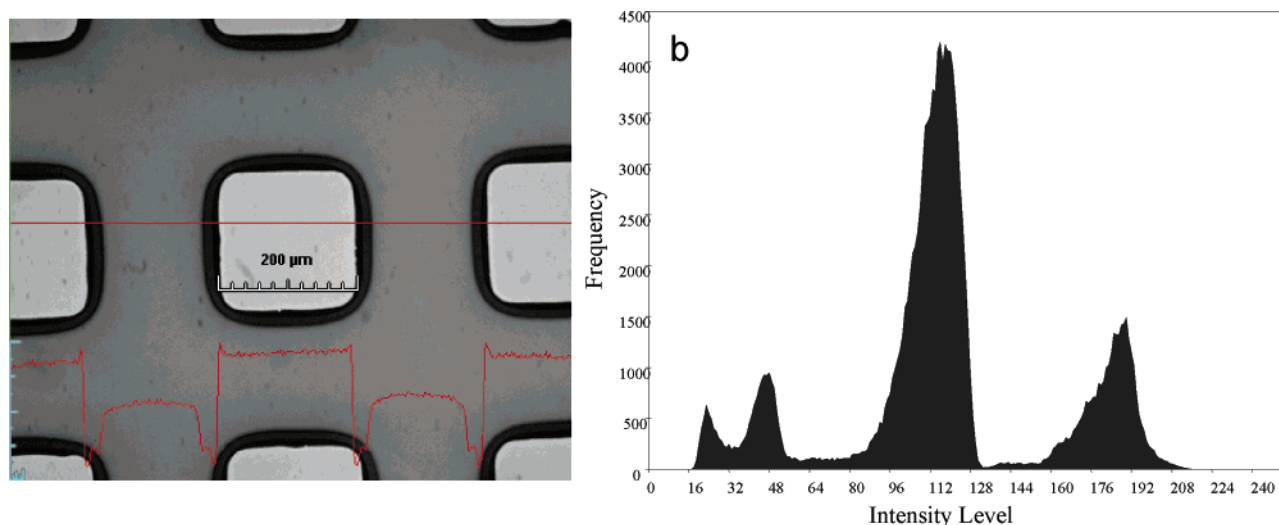
**Figure 4.** Epifluorescence image and corresponding intensity histogram of a supported phospholipid bilayer (1% TR-DHPE and 99% POPC) formed by vesicle fusion over patterned OTS on 100 nm thick $SiO_2/Si$ substrate. Four regions of differing intensity are visible both in the image and in the histogram. The two regions of the lowest intensity are in the moat region.

itself. The limiting patternable sizes[54] and densities have not yet been determined, but should be limited by a combination of factors influencing the photopatterning parameters (e.g., the sample-to-mask alignment efficiency and edge effects) and vesicle spreading parameters. When we repeated the experiment for various patterning shapes, features ($>5$ $\mu$m) resulted in comparable relief structures. Using various fluorophores (e.g., Texas Red, NBD, rhodamine, and DiIC18-labeled DHPE lipid−probes), the spontaneous pattern formation in lipid morphologies was independent of the nature of the fluorophores, except for DiIC18 where the dye molecule tends to migrate to the edge of the moat area. *Because DiIC18 prefers a gel-like lipid environment,[55] we conclude that the DiI migration toward the edge is suggestive of a denser lipid environment at the boundaries of the contiguous lipid phases. These results are in disagreement with a recent molecular simulation where it was postulated that the bilayer at the edges is more fluid.[56]* Several phospholipids, including DMPC, DLPC, and POPC, lead to spontaneous pattern formation, confirming this process is independent of the phase state of the lipid and chain unsaturation of the lipids used. Moreover, comparable results were obtained when bilayer preparation employed Langmuir−Blodgett or vesicle fusion methods.

The stability of the patterned features was confirmed by observing the epifluorescence emission from samples stored under water or aqueous buffer for several days. A daily examination of the fluorescence patterns over a period of 1 week revealed the expected diminution of fluorescence intensity, whereas the sizes, intensity ratios, and relative positions with respect to the substrate and among the features remained intact, indicating a long-term stability of the patterns.

**Fluorescence Photobleach Recovery.** A simple adaptation of the widely used fluorescence photobleach recovery method was used to determine the fluidity of phospholipid layers in the hydrophilic and the hydrophobic parts of the initial OTS template. Selected frames ($t = 0$ s, 1, 2.5, and 5 min) from a

time-lapse sequence of images obtained during microscopy-based fluorescence photobleach recovery measurements for a POPC bilayer and monolayer fused on a patterned OTS substrate containing approximately a 1 mol % TR-DHPE probe are shown in Figure 6. Immediately following the photobleaching, a relatively sharp circular feature indicative of bleached fluorophores is seen (Figure 6a). As a function of time, the fluorescence intensity within the spot is observed to gradually recover, ultimately leading to a uniform, lowered intensity across the image window. This behavior is indicative of the translational mobility of the fluorophore within the contiguous parts of the bilayer/monolayer structure.[38] Our observations of such fluorescence recovery, illustrated in Figure 6, for both the high-intensity square regions and the lower-intensity background regions of the samples, confirm the essentially two-dimensional fluidity of each of the two fluorescent regions. Attempts to conduct FPR measurements in the moat region were unsuccessful, further suggesting the absence of any measurable fluorescence intensity and lack of fluid lipid layer in that region. Such fluidity of the lipid was observed to persist uniformly in all areas of the lipid layers, including in the close proximity of the moat regions.

Following an approximation derived by Yuegbride and Foster,[40] we estimate the probe diffusion coefficient, $D$, to be $\sim 0.6$ $\mu$m$^2$/s by averaging $D$ over two different positions on different samples for the bilayer regions (one in the center of a corralled bilayer and one closer to the moat region) at room temperature conditions. These values are well within the range of 0.5−5 $\mu$m$^2$/s reported for fluid bilayers in previous studies under similar ambient conditions.[39] Similarly, the probe diffusion coefficient, $D$, for the monolayer region estimated from diffusion measurements over two different positions on different samples for the monolayer (one position equidistant from the bilayer regions and one close to the moat region) was $\sim 0.3$ $\mu$m$^2$/s. *Given large errors (0.5 $\mu$m$^2$/s) inherent in the diffusion constant estimations from our objective-based FPR measurements, we cannot conclusively infer if there was a systematic difference in the fluidity of the lipid monolayer from that of the bilayer.* Quantitative measurements are underway in our laboratory to

---

(54) When hydrophilic regions were smaller than 5 $\mu$m in photopatterned silane monolayers, the vesicle fusion process resulted in the formation of an epifluorescence layer in the hydrophobic background alone. We are currently investigating the smallest patternable sizes.
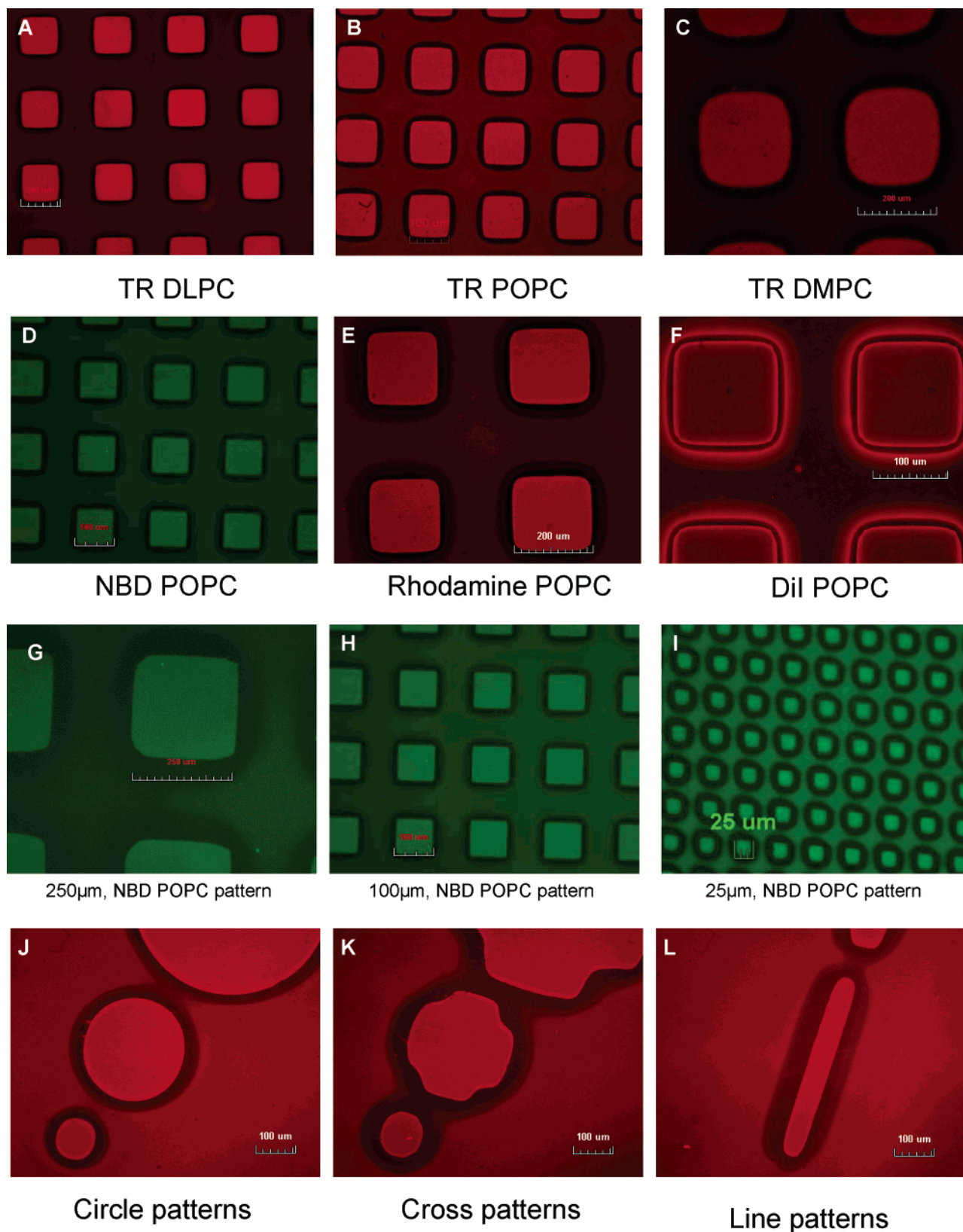
**Figure 5.** Epifluorescence images of supported bilayers on patterned OTS surfaces obtained using selected lipids, fluorophores, and pattern sizes and shapes: (A) DLPC, (B) POPC, and (C) DMPC doped with 1 mol % Texas Red−DHPE; images in D−F show POPC bilayers doped with trace amounts of NBD-DHPE, rhodamine-DHPE, and DiIC18 probes; G−I show NBD-DHPE-doped POPC bilayers showing 250, 100, and 25 $\mu$m feature sizes, and J−L images confirm shape independence.

discriminate between lipid mobility in the hydrophilic voids versus the OTS surface. Taken together, these estimates suggest that the lipid layers in both the UV-exposed hydrophilic parts and the UV-protected hydrophobic parts of the initial OTS template retain their overall fluidity. We note that the objective-based illumination for fluorescence recovery measurements used

## Bilayer FPR
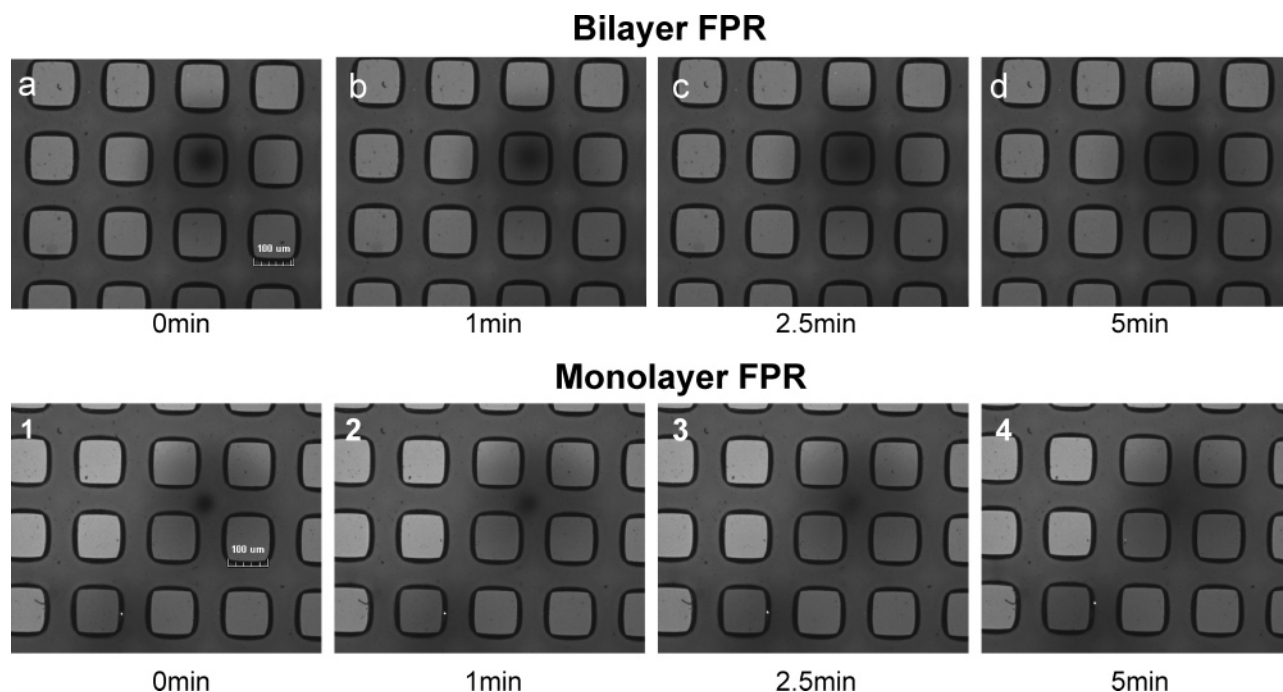


## Monolayer FPR



**Figure 6.** Selected frames from fluorescence photobleaching recovery image sequence. The first set of images (a–d) confirm fluidity in the corralled bilayer, and the second set of images (1–4) show the monolayer fluidity characteristics (see text for details).

here is, at best, semiquantitative and makes it difficult to make precise determination of fluorophore diffusion coefficients. This is because relatively long exposure periods were required for photobleaching (~2−5 min depending on the age of the lamp). Molecular motions of fluorophores during the photobleach period lead to some unaccounted variations in the fluorescence intensities.

To determine if the molecular transport occurred between the *bilayer* and the *monolayer* regions of the fluorescent patterns across the moat, we bleached the entire region of the brighter (and darker) fluorescence. These data are shown in Figure 7. These simple measurements revealed that there was no measurable recovery of the bleached regions, indicating that the bleached fluorophores were confined to the corralled brighter (or the darker) regions. These data establish unambiguously that the lipid contiguity is broken at the moat region, and that the molecules within the square region are isolated, albeit fluid within the contiguous feature area, from the surrounding regions.

Taken together, the fluorescence photobleach recovery measurements above confirm the formation of two fluid lipid layers that are discontinuous at the fluorescence-free border or the moat. We further conclude that the brighter regions correspond to contiguous fluid bilayers, whereas the lighter regions represent half-bilayers (monolayers) supported on a hydrophobic surface.

**Imaging Ellipsometry.** A typical two-dimensional map of the ellipsometric angle, Δ, and a corresponding thickness map are shown in Figure 8a and b, respectively. The images show three well-separated regions of relatively uniform Δ values. In particular, the data immediately show the presence of a narrow *fence or* moat separating the square blocks from the surrounding areas. The ellipsometric angle values presented in Figure 8a for the background and the corralled square are comparable with those for the square corrals at slightly, but consistently, higher values. The moat separating the two regions is at significantly higher Δ values, indicating markedly different thickness morphology in that region. A comparison with the sample history

### Corralled Bilayer



### Corralled monolayer
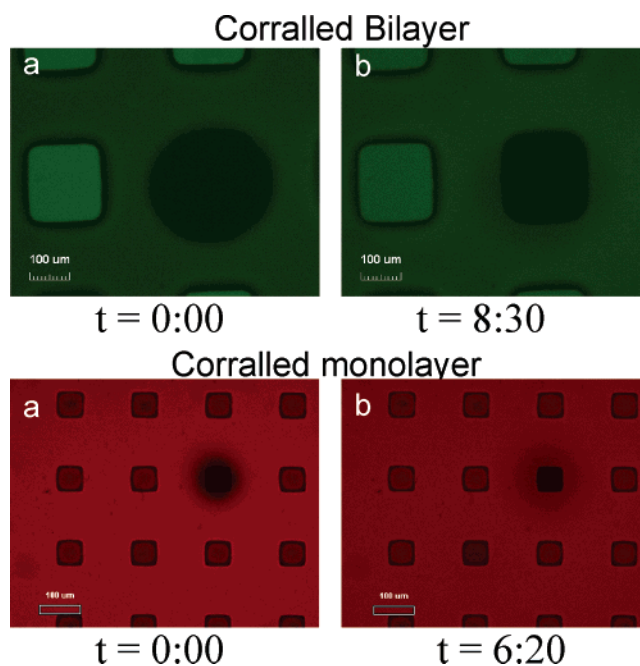


**Figure 7.** In the first set of images, 3% NBD-DHPE and 97% POPC was spread over patterned OTS on a glass coverslip, which resulted in corralling of the bilayer in a matrix of monolayer. The first image (a) was taken directly after photobleaching in and around the corralled bilayer. The second image (b) is the last in a series of images taken over 8 min and 30 s. In the second set of images, the monolayer has been corralled in a matrix of bilayer. Lipid here is 1% Texas Red DHPE and 99% POPC. The first image (c) was taken after photobleaching in and around the corralled monolayer. The second image (d) is the last in a series of images taken over 6 min and 20 s. The bleached regions within the rim do not recover. In both cases, inner and outer regions were fluid.

suggests a strong correlation between the patterns in ellipsometric angles and the pattern of UV illumination during photopatterning of the OTS monolayer and the subsequent fluorescence patterns observed upon spreading of phospholipid vesicles (see above). These correlations establish that the
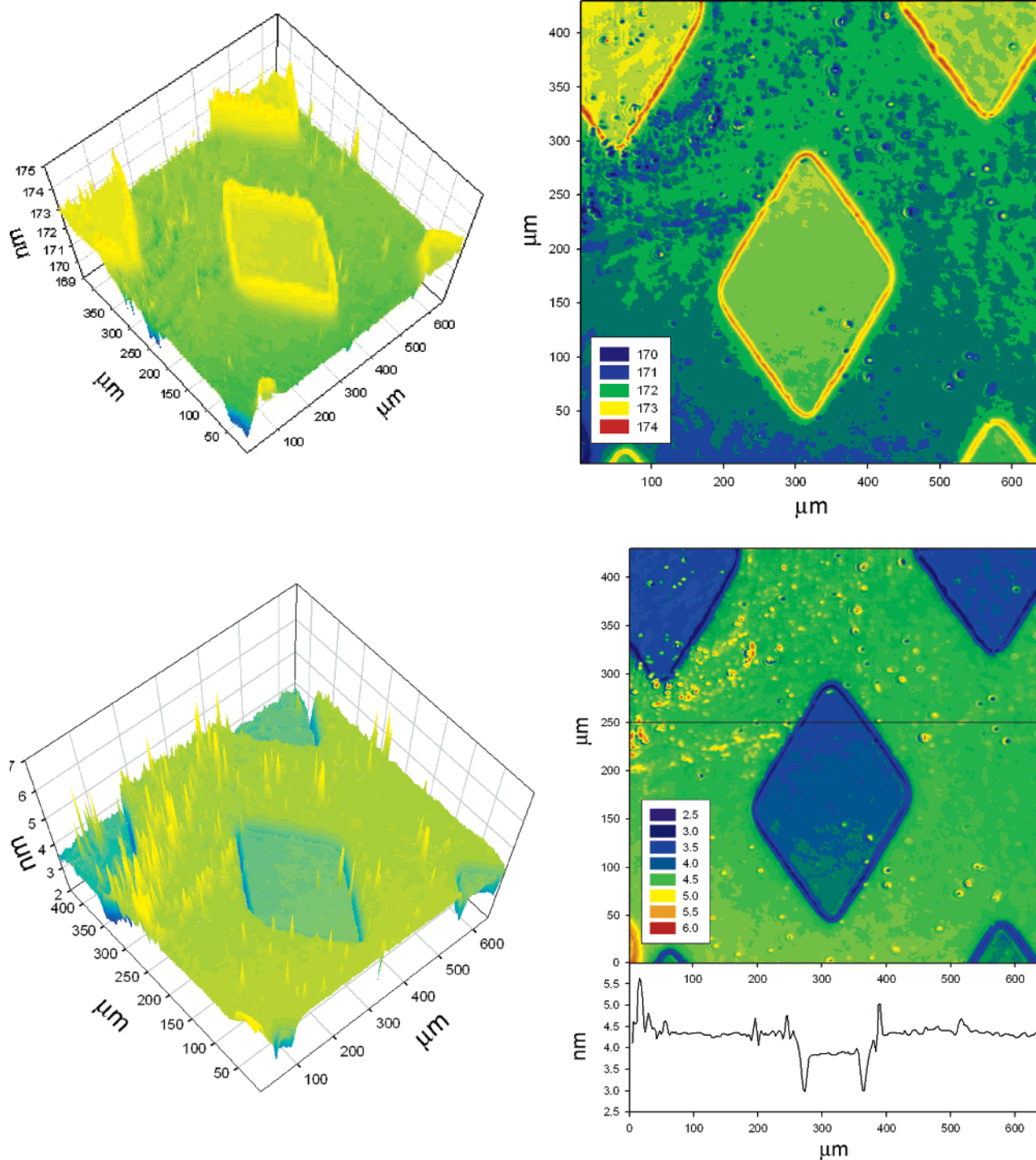
**Figure 8.** (a) An ellipsometric contrast image revealing the spatial variation in ellipsometric angle, $\Delta$ for a UV-patterned OTS film upon which a 3% NBD-DHPE and 97% POPC vesicle solution is fused. (b) Thickness map for the data is shown in Figure 8a. The inset shows a section in the direction of the black arrow. The bilayer has an average thickness of 3.8 nm *without SiO_x headgroup*, and the lipid monolayer with the OTS film has an average thickness of 4.6 nm.

fluorescence patterns in the lipid layer noted earlier can be attributed to the differences in the film thickness morphologies. Specific changes in the average ellipsometric angle, $\Delta$, relative to a bare-patterned OTS surface imaged under water in a wet cell (data not shown), for the surrounding and the square regions, are 174 and 176° for the patterned OTS substrate and 172.5 and 173.5° for the lipid fused on the patterned OTS substrate, respectively. These changes are consistent with the deposition of lipid layers in these regions. By contrast, there is little change

in the $\Delta$ values for the moat region (average of 174°, similar to the $\Delta$ value obtained for the OTS monolayer), suggesting little adsorption of lipid in that region.

A particularly informative way to interpret ellipsometric angles is to derive spatial variations in optical thicknesses from the ellipsometric contrast images. Figure 8b plots these values. Also shown, as an inset is a cross-section along the *y*-axis. These data indicate that thicknesses of the bilayer in the square is 38 ($\pm$3) Å and the surrounding regions are at 46 Å. The thickness
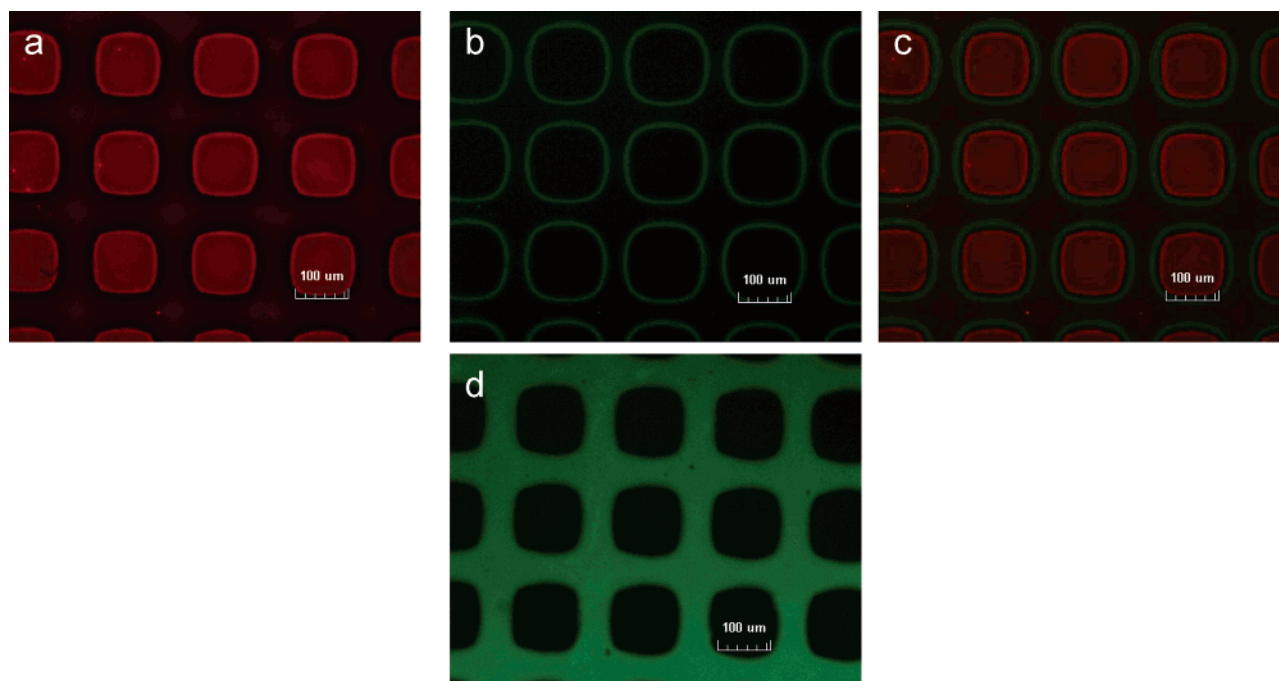
**Figure 9.** (a) A red channel image representing a membrane pattern obtained by spreading 1% Texas Red and 99% POPC on patterned OTS with 100 $\mu$m feature. (b) A green channel image acquired after incubating the sample represented in 9a with FITC−BSA protein forming a green rim. (c) A composite, red and green channel, image of membrane pattern with FITC−BSA. Epifluorescence image in 9d is a control experiment showing the incubation of FITC−BSA with patterned OTS not incubated with vesicle solutions.

in the moat region, however, was between 25 and 30 Å. In the square corrals, since we expect the thickness of the SiO$_x$ cluster to be ∼2−3 Å, the remaining 38 Å can be attributed to the *POPC bilayer.* This value is in good agreement with a range of values reported previously between 37−55 Å for a well-formed POPC bilayer derived using neutron reflectivity, X-ray, and NMR measurements.[57−59] The organic layer thickness in the background region indicates the overall thickness due to the OTS layer and the lipid layer. Since the OTS thickness is estimated to be 26 Å, the remaining 20 Å can be attributed to the lipid monolayer. This value matches closely with the formation of a single monolayer onto the OTS layer, also consistent with lower fluorescence intensities for the region and with several previous studies which establish that the hydrophobic surfaces promote vesicle spreading to form half-bilayers or single monolayers. In sum, the square regions and the surrounding areas of the patterns are topographically comparable in ellipsometric heights above the SiO$_2$/Si substrate, whereas the moat region represents a depression of about 28 Å. On the basis of the model of monolayer formation in the hydrophobic part and bilayer formation in the hydrophilic part, the evidence above is consistent with the absence of lipid molecules at the rim of the OTS monolayer.

**Protein Adsorption Characteristics.** To better characterize the nature of the lipid-free moat region, we explored the possibility of adsorbing secondary species within the moat regions. Two classes of experiments were performed. We first explored if comparable or distinctly different vesicles would

access the moat region. These experiments yielded no measurable changes in the fluorescence intensities or ellipsometry images of the initial lipid patterns, suggesting long-term lipophobic character of the moat region. Next, we explored the ability of soluble proteins[60−63] to access and adsorb into the moat region.[64,65] We used bovine serum albumin (BSA) and streptavidin. *Prior to incubation, substrates were transferred from water to PBS. Proteins were then added dropwise from their stock solutions in PBS (pH 7.2) to give final concentrations of 1.25 and 0.5 μg/mL for FITC−BSA and FITC−streptavidin, respectively. Incubation times were at least 20 min for FITC−BSA and 2 h for FITC−streptavidin.* To enable examination by simple epifluorescence measurements, both proteins were labeled with FITC. Representative images of *FITC−BSA* are shown in Figure 9a−c. The images reveal significant adsorption in the exterior moat region, whereas little adsorption was evident in the interior moat closer to the bilayer edge, as judged by the appearance of green fluorescence due to FITC.[66] *FITC−streptavidin was observed to exhibit similar behavior (data not shown).*

These results unambiguously show that both the square regions, attributed to lipid bilayer morphology, and the surrounding areas, assigned to lipid monolayers, were resistant to *any* adsorption by the proteins. These results are in good

(55) Spink, C. H.; Yeager, M. D.; Feigenson, G. W. *Biochim. Biophys. Acta* **1990**, *1023*, 25.
(56) Kasson, P. M.; Pande, V. S. *Biophys. J.* **2004**, *86*, 3744.
(57) Salditt, T.; Vogel, M.; Fenzl, W. *Phys. Rev. Lett.* **2003**, *90*.
(58) Kucerka, N.; Kiselev, M. A.; Balgavy, P. *Eur. Biophys. J. Biophys. Lett.* **2004**, *33*, 328.
(59) Nagle, J. F.; Tristram-Nagle, S. *Biochim. Biophys. Acta Rev. Biomembranes* **2000**, *1469*, 159.
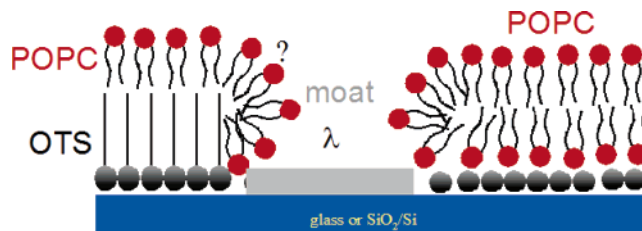
(60) Malmsten, M. *Colloids Surf., A* **1999**, *159*, 77.
(61) Malmsten, M. *J. Colloid Interface Sci.* **1995**, *172*, 106.
(62) Glasmastar, K.; Larsson, C.; Hook, F.; Kasemo, B. *J. Colloid Interface Sci.* **2002**, *246*, 40.
(63) Ross, E. E.; Spratt, T.; Liu, S. C.; Rozanski, L. J.; O'Brien, D. F.; Saavedra, S. S. *Langmuir* **2003**, *19*, 1766.
(64) Norde, W.; Macritchie, F.; Nowicka, G.; Lyklema, J. *J. Colloid Interface Sci.* **1986**, *112*, 447.
(65) Ying, P. Q.; Yu, Y.; Jin, G.; Tao, Z. L. *Colloids Surf., B* **2003**, *32*, 1.
(66) In all experiments, we noted a region of the moat between the moat/hydrophilic interface where protein adsorption was negligible. We believe this to reflect a partially hydrophilic nature of the sample surface in immediate vicinity of the pattern edges presumably via partial lipid oxidation.

agreement with a now well-established observation that fluid lipidic surfaces are resistant to adsorption by many soluble proteins.[60-63] The adsorption of proteins in the moat region at the interface between the lipid bilayer and the lipid monolayer further reflected its fine structure. The interior moat, closer to the bilayer edge, was lipid resistant, but the exterior moat showed uniform protein adsorption. These results are consistent with our suggestion that the penumbral blurring in the photopatterning renders the pattern edges topochemically rough. As a control experiment, we also exposed samples consisting of patterned OTS surfaces, prior to exposure to lipid vesicle solution, to FITC−BSA and FITC−streptavidin proteins. *Representative FITC−BSA data are presented in Figure 9d.* FITC green fluorescence emission and, hence, adsorption almost exclusively on the unilluminated OTS layer is observed. By contrast, the hydrophilic silica regions, obtained by photopatterning of OTS (see above), remained resistant to protein attachment. *Again, FITC−streptavidin exhibited similar behavior.* Several previous studies have suggested that such topochemically rough surfaces promote protein adsorption,[67,68] such as observed here.

## Discussion

**Structural Summary.** All the data presented in this paper can be reconciled in terms of a unifying picture of coexisting lipid morphologies at photochemically patterned OTS monolayers. At least three regions of discernibly different thickness morphologies for the lipid phases coexist in UV-patterned OTS monolayers: (1) fluid phospholipid bilayers in the UV-illuminated regions; (2) fluid phospholipid monolayers in the unilluminated masked portions; and (3) the lipid-free gap or moat in the interface region at the boundary of the illuminated and the masked parts of the OTS monolayer. Several samples displayed a fourth ill-defined region of low lipid density at the interface between the masked portion of the OTS sample and the moat. We call this region an exterior moat. These lipid morphologies further display a correspondence with the topochemical character and the *interfacial* energy. The hydrophilic parts of the substrate support the formation of a fluid bilayer, and the hydrophobic parts of the substrate facilitate monolayer assembly. The interface between the hydrophilic and the hydrophobic regions or the moat of the substrate exhibits a more complex lipid assembly. The interface itself consists of at least two additional regions consisting of a nonfluid lipid phase closer to the hydrophobic edge in the exterior moat and a lipid-free moat in the vicinity of the hydrophilic edge of the substrate pattern. This overall structure is consistent with the features implied by the schematic in Figure 10.

Formation of uniform lipid layers in each, the hydrophilic and the hydrophobic parts of the sample, was established by the uniform fluorescence intensities obtained for the lipidic layers (Figure 3). The conclusion is further supported by spatially resolved optical ellipsometric measurements which reveal a uniform film thickness with less than 5% spatial variations (Figure 8b). Furthermore, the precise values of optical thicknesses estimated using ellipsometric data allowed a direct discrimination of the two layers. Assigning a cluster thickness

(67) Sethuraman, A.; Han, M.; Kane, R. S.; Belfort, G. *Langmuir* **2004**, *20*, 7779.
(68) Cacciafesta, P.; Hallam, K. R.; Watkinson, A. C.; Allen, G. C.; Miles, M. J.; Jandt, K. D. *Surf. Sci.* **2001**, *491*, 405.

**Figure 10.** A schematic diagram for the proposed morphology of lipid layers on patterned OTS surfaces (see text for details). The boundary between the monolayer and the bilayer region was difficult to characterize, depicted as an ill-defined, L, region. Our data suggest a chemically roughened surface of intermediate hydrophilicity which fosters some lipid attachment near the hydrophobic boundary and a lipid-free inner moat near the hydrophilic boundary (see text for details.)

of ~3 Å for residual $SiO_x$ in the hydrophilic parts of the sample yielded a film thickness of 38 Å for the lipid films. In the hydrophobic parts of the sample, the assignment of ~26 Å to the OTS film layer estimated the lipid thickness to be ~20 Å. These values agree well with the full and half-bilayer morphologies (see Results above) in the hydrophilic and the hydrophobic parts of the sample. This inference is further supported by the observations of almost double fluorescence intensities in the hydrophilic parts of the sample relative to those of the hydrophobic parts of the pattern (Figure 3). The lipid layers were two-dimensionally contiguous fluids, as shown clearly by the simple fluorescence photobleach recovery measurements (Figure 6). Our preliminary quantitation efforts yielded consistent differences in the fluidity of the lipid layers supported on the hydrophobic and the hydrophilic parts of the substrate. More rigorous measurements will be necessary to establish the effects of interlayer couplings on quantitative differences in probe mobilities within the lipidic monolayer and bilayer phases. Such studies are currently underway in our laboratories.

A notable feature of the film architecture was the existence of the moat region at the interface between the monolayer and the bilayer morphologies. Note also that the moat regions were observed in several experimental configurations independent of the pattern shapes, sizes, types of lipids, or fluorophores used for visualization. The moat region (including the exterior moat) was several micrometers in width. The exact width of the moat region varied from sample to sample and appeared to be controlled by the spacing and alignment between the mask and the sample during the photopatterning of the silane monolayers. These results suggest the primary role of edge effects or penumbral blurring in the mask photolithography of the parent OTS monolayer. The exterior moat or the interface close to the monolayer edge systematically showed low, but nonvanishing, fluorescence emission that did not recover in photobleach experiments. We believe these data suggest the presence of low surface densities of lipids either as adsorbed free lipids or as unfused vesicles. This region was further found to be accessible by FITC-labeled bovine serum albumin and streptavidin proteins in subsequent incubations. By contrast, the edge of the interface closest to the fluid lipid bilayers was free of fluorescence in all experiments described here, indicating little adsorption of lipids in this region, which was also inaccessible by proteins. Thickness estimations using ellipsometry (Figure 8) did not reveal any measurable topographic differences in this fine structure, further consistent with low densities of the lipidic phases in these regions.

The unique character of the lipidic morphologies obtained using photopatterned silane monolayers in this study has many practical ramifications. Below, we briefly discuss some useful applications of this construct. First, the spontaneous separation of the fluid bilayer regions from the fluid monolayer regions by the moat interface provides a simple but elegant method to compartmentalize the fluidity of lipid bilayers. Such constructs are potentially useful for parallelizing many assays for membrane targets, for example, in designing biosensor arrays. Second, the ability of the bilayer region to embed bilayer spanning long molecules (e.g., tethers used for biosensor constructs) and potentially membrane proteins (e.g., ion channels) should prove to be useful in fabricating microarrays for functional proteins. A particularly attractive feature of our construct, in this regard, is the lipidic character of the background separating the bilayer patches, which is resistant to nonspecific protein adsorption. Third, the bilayer/monolayer composite construct should prove to be useful in exploring fundamental biophysical questions about the interleaflet cooperativity in membrane assembly, dynamics, and function. Examples include (1) probe and molecular partitioning preferences with respect to the bilayer leaflet and (2) coordination between the leaflets in determining the nature of phase separations in multicomponent membranes. A desirable feature of our patterns, in this regard, is to facilitate side-by-side measurements on monolayer and bilayer lipid media in single incubations. Fourth, the highly local response of vesicle fusion mechanisms to surface topochemical character and surface energies is attractive in assaying surface heterogeneities of the substrates over large areas. Microscopic defects of topochemical character on the substrate surface can be easily probed by simply exposing these surfaces to vesicular solutions and examining the lipid morphologies. Fifth, the protein adsorption data illustrate the usefulness of the approach in designing predetermined patterns of proteins and using the lipid phase as a surrounding matrix or a sacrificial resist layer.

**Implications for Vesicle Spreading Mechanisms.** It is well-known that hydrophilic substrates allow vesicle spreading that results in two-dimensionally fluid phospholipid bilayers. By contrast, hydrophobic surfaces yield single monolayers of lipids. It is generally believed that the fusion of the phospholipid vesicles at solid surfaces is governed by a combination of electrostatic, van der Waals, hydration, and steric forces.[34] On hydrophilic surfaces (e.g., silica), the preponderance of electrostatic and van der Waals interactions dominates the vesicle fusion process, whereas on hydrophobic surfaces, the minimization of the interfacial free energy via a coupling between the hydrophobic surface and the hydrophobic tail of the lipid molecules guides the self-assembly, producing single lipid monolayers. It has also been previously observed that topologically roughened surfaces impede vesicle spreading.[34] Results presented here suggest a strong spatial and local correlation between the substrate topochemical character and the vesicle spreading behavior. Microscopic spatial variations in surface characteristics (and/or surface energies) are shown to result in spontaneous changes in the spreading behavior to produce complex, coexisting lipid morphologies on single substrates.

In this vein, it is useful to compare the results of our study with those reported by Nissen and co-workers[69] on the spreading of lipids from a large reservoir onto mixed hydrophilicity surfaces. There, it was shown that the lipid spreading does not occur on hydrophobic "defects", and the advancing lipid front in the hydrophilic surroundings showed relaxation behavior reminiscent of the broadly investigated problem of the spreading of nonreactive fluids on chemically structured surfaces.[70,71] Our results appear to contrast Nissen et al.'s observations by indicating that vesicles from their dilute solutions assemble on both hydrophilic and hydrophobic surfaces by mechanisms that are controlled by the local interplay of interactions between the substrate and the vesicles. This apparent contradiction highlights a key difference between the popular vesicle fusion methods, such as that used in the present study, and the spontaneous spreading of vesicle solution on chemically heterogeneous substrates. The fluid invasion conditions during spontaneous spreading, such as in experiments, reported by Nissen et al.[20,69] only selectively wets the hydrophilic regions of a chemically patterned substrate surface, thereby preserving a single self-assembly mechanism. By contrast, most widely used methods for vesicle fusion employ direct incubation of substrates, such as by substrate immersion into the vesicle solution, forced spreading of vesicle solutions between two planar substrates, or by Langmuir−Blodgett techniques. In all of these techniques, the substrate is fully wetted by the vesicle solution. In these cases, our results illustrate that the local control of vesicle spreading mechanisms by the substrate characteristics results in complex lipid morphologies.

## Conclusions

Using photochemically patterned self-assembled monolayers of *n*-octadecylsiloxanes, we produced periodic arrays of square hydrophilic domains separated from hydrophobic surroundings. Exposing these patterned surfaces to a solution of small unilamellar vesicles of phospholipids and their mixtures resulted in a complex lipid layer morphology epitaxially reflecting the underlying pattern of substrate topochemical character. The hydrophilic square regions of the photopatterned OTS monolayer reflected lipid bilayer formation, and the hydrophobic OTS residues supported lipid monolayers. We further observed the presence of a complex moat region at the interface between the lipid monolayer and bilayer morphologies spontaneously corralling the fluid bilayers. The lipid-free region of the moat was resistant to subsequent vesicle adsorption or protein adsorption. The exterior moat in the vicinity of the hydrophobic edge of the substrate, on the other hand, was determined by the shadow-edge effects in the photopatterning and allowed adsorption of BSA and streptavidin proteins. These results provide a basis for the construction of complex biomembrane models, which exhibit fluidity barriers and differentiate membrane properties based on correspondence between lipid leaflets. We also envisage the use of this construct where two-dimensionally fluid, low-defect lipid layers serve as sacrificial resists for the deposition of protein and other material patterns. Furthermore, the study also highlights the highly local role of topochemical substrate heterogeneities in determining the vesicle spreading behavior at solid surfaces.

**Post-Script Foot Note.** While this paper was in review, Lenz and co-workers (Lenz, P.; Ajo-Franklin, C.; Boxer, S. G.

(69) Nissen, J.; Jacobs, K.; Radler, J. O. *Phys. Rev. Lett.* **2001**, *86*, 1904.
(70) Lenz, P.; Lipowsky, R. *Phys. Rev. Lett.* **1998**, *80*, 1920.
(71) Sharma, A.; Reiter, G. *Phase Transitions* **2002**, *75*, 377.

Langmuir **2004**, 20, 11092−11099) reported a comparable finding of coexisting lipid morphologies on a patterned wettability, plasma-oxidized poly(dimethyl)siloxane (PDMS) substrate. Remarkably, they observe lipid morphologies including lipid-free gap region in topochemically rough edges similar to the work reported here, albeit the mechanisms of surface roughening appear to be very different. Many control experiments in their study suggested that the material transport at the surface of the PDMS during plasma oxidation in conjunction with the exposure-dependent plasma oxidation of masked PDMS substrates resulted in the boundary regions of intermediate wettability. In our study, the topochemical roughening of the boundary between the mask and the OTS-covered substrates in UV photolithography appeared independent of the exposure time, but depended critically on the distance between the mask and the sample due to the penumbral effects of photopatterning (see text for details).

**Supporting Information Available:** Additional figures. This material is available free of charge via the Internet at http://pubs.acs.org.

JA043439Q